ELSEVIER

Chemical Engineering Journal 69 (1998) 85–91

Chemical Engineering Journal

Modelling of liquid circulation velocity in concentric-tube airlift reactors

M. Gavrilescu [a,*], R.Z. Tudose [b]

[a] Chemical–Pharmaceutical Research Institute, Research Center for Antibiotics, 6647-Valea Lupului No. 1, Jassy, Romania

[b] Technical University of Jassy, Faculty of Industrial Chemistry, Department of Chemical Engineering, Mangeron Street 71, 6600 Jassy, Romania

Received 16 December 1996; accepted 11 August 1997

Abstract

A mathematical model for riser liquid superficial velocity in a concentric-tube airlift reactor is proposed. The model is based on an energy balance incorporating acceleration coefficients to quantify deviations from ideal flow. The acceleration coefficients at the draft-tube and downcomer entrance are determined experimentally, based on static pressure profile measurements. The model could predict liquid velocities over a broad range, including an almost 50-fold variation of liquid circulation velocity and a four-fold change in reactor height. The model predictions agreed with the measurements to within ±28%.

Keywords: Liquid circulation velocity; Airlift reactor

1. Introduction

Airlift reactors have attracted much attention in the chemical industry and in biotechnology because of their hydrodynamic characteristics, especially their readily controllable liquid circulation rates.

Liquid circulation originates from the difference in bulk densities or static heads between the gas-sparged section (riser zone) and the unsparged zone (downcomer). This induced fluid circulation is a major design characteristic of airlift reactors because it determines the residence time of the liquid in various zones and controls the reactor's performance (mass transfer, heat transfer, mixing, turbulence) [1–5]. Irrespective of application, the prediction of the gas-induced circulation of liquid is a key aspect of reactor design.

Models for predicting the induced liquid circulation rate have been described in the literature [2,4,6–9]. Such models are based usually on momentum or energy balances.

In this work, an energy balance is applied to concentric-tube airlift reactors for developing a mathematical model for liquid circulation velocity, taking into account the energy losses along the total circulation loop, especially in the bottom and top sections. Such losses are caused by apparent contraction of the flow cross sections, and quantified by the acceleration coefficients that are estimated using measurements of static pressure profiles.

2. Liquid circulation model

The difficulties in evaluating the energy loss along the total circulation loop in the airlift reactor stem partly from the complex nature of the flowing gas–liquid mixture and partly from the difference in the factors controlling the energy loss process, at least initially since the process always ends with viscous dissipation in particular sections of the loop. Specifically, there are two contributions: (1) in the riser and downcomer, the energy losses occur due to viscous dissipation localized in regions of intense shear, e.g., along the column walls; (2) in the top and bottom sections, the energy losses are caused by expansion/contraction of the two-phase flow.

Finally, the liquid circulation rate in concentric-tube airlift reactors is determined by the balance between the hydrostatic pressure driving force due to the differential gas holdup between the riser and the downcomer and the flow resistances along the loop, especially at the ends of the draft-tube.

The following assumptions are made for the energy balances around the bottom and top sections, and they relate, in particular, to interactions between the phases: the contribution of the backflow velocity field induced in the liquid phase by the relative motion of the bubbles is totally ignored [10]; the energy losses associated with the relative motion between the gas and liquid phases including the bubble-wake effect, often incorporated into energy balance models [7,11] are not taken into account in this work. This is mainly because our interest in the bottom and top sections of the airlift reactors—not the straight vertical sections where the relative or slip

* Corresponding author.

1385-8947/98/$19.00
PII S1385-8947(97)00100-9

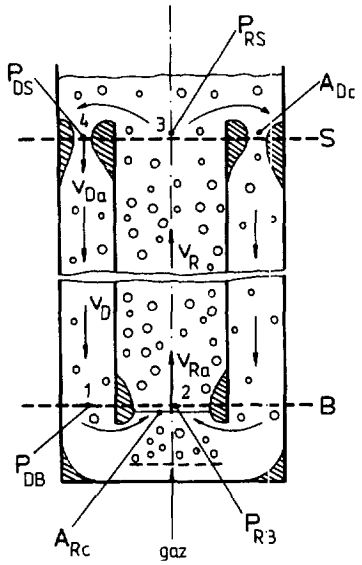

Fig. 1. Conceptual flow scheme in concentric-tube airlift reactors (gas sparged in draft-tube; the hatched regions indicate the contracted flow sections, where flow acceleration occurs).

velocities of the bubbles in the liquid flow are significant. These effects can be taken into account in the empiricism inherent to the description of the pressure drops [12]; the radial velocity distribution of the gas–liquid flow near the elbow and separator regions are uniform; the volume change of gas phase associated with static pressure variation follows the isothermal expansion/contraction of an ideal gas [12].

Considering the conceptual flow scheme in the concentric-tube airlift reactor as presented in Fig. 1, there are changes of the cross-sectional areas for liquid circulation at both ends of the draft-tube. These changes alter local values of the liquid velocity. The changes in linear velocity should be accompanied by changes in static pressure so as to maintain the energy balance. The flowing liquid turns through 180° at the entrance to the draft-tube and annulus. As a result, the pressure and velocity fields will be subject to entrance effects reducing the effective flow area [13], and producing liquid acceleration. These accelerations are the result of an apparent diminishing of flow cross sections (Fig. 1).

This behaviour was modelled through a simple energy conservation model in the form of Bernoulli's equation, in the sections B and S, (Eqs. (1) and (2)), together with the pressure balance in riser and downcomer (Eqs. (3) and (4)) and the equations of continuity at both ends of the draft-tube (Eqs. (5) and (6)).

In Bernoulli's equation, applied at each end of the draft-tube, the linear velocities of the liquid phase at the contracted entrances to the riser and downcomer (sections B and S) were related to the effective linear velocities, $v_{R\alpha}$ and $v_{D\alpha}$, respectively.

$$\frac{1}{2}\rho v_D^2 + P_{DB} = \frac{1}{2}\rho v_{R\alpha}^2 + P_{RB} \tag{1}$$

$$\frac{1}{2}\rho v_R^2 + P_{RS} = \frac{1}{2}\rho v_{D\alpha}^2 + P_{DS} \tag{2}$$

The terms for gas–liquid interaction and viscous energy dissipation were neglected.

Neglecting wall friction, the vertical pressure gradient is related to the gas holdup in riser and downcomer, respectively, by:

$$P_{DB} - P_{RB} = \rho g(1-\varepsilon_{GR})H_d \tag{3}$$

$$P_{RS} - P_{DS} = \rho g(1-\varepsilon_{GD})H_d. \tag{4}$$

Continuity equations at each end of the draft-tube may be expressed as:

$$(1-\varepsilon_{GD})A_D v_D = (1-\varepsilon_{GR})A_{Rc}v_{R\alpha} \tag{5}$$

$$(1-\varepsilon_{GR})A_R v_R = (1-\varepsilon_{GD})A_{Dc}v_{D\alpha}. \tag{6}$$

Combination of Eqs. (1)–(6) leads to the implicit expression of the energy balance.

$$2gH_d(\varepsilon_{GR}-\varepsilon_{GD}) = v_R^2\left[\frac{(1-\varepsilon_{GR})^2}{(1-\varepsilon_{GD})^2}\frac{A_R^2}{A_{Dc}^2} - 1\right] + v_D^2\left[\frac{(1-\varepsilon_{GD})^2}{(1-\varepsilon_{GR})^2}\frac{A_D^2}{A_{Rc}^2} - 1\right] \tag{7}$$

The linear liquid velocities in the riser and downcomer, v_{LR} and v_{LD}, respectively, are related to the corresponding superficial velocities as follows:

$$v_{SLR} = v_{LR}(1-\varepsilon_{GR}) \tag{8}$$

$$v_{SLD} = v_{LD}(1-\varepsilon_{GD}). \tag{9}$$

Furthermore, the continuity equation for the liquid flow between the riser and the downcomer can be written as:

$$A_R(1-\varepsilon_{GR})v_{LR} = A_D(1-\varepsilon_{GD})v_{LD}. \tag{10}$$

By considering Eqs. (8)–(10), Eq. (7) becomes:

$$2gH_d(\varepsilon_{GR}-\varepsilon_{GD}) = v_{SLR}^2 A_R^2\left[\frac{1}{(1-\varepsilon_{GR})^2 A_{Rc}^2} - \frac{1}{(1-\varepsilon_{GD})^2 A_D^2} + \frac{1}{(1-\varepsilon_{GD})^2 A_{Dc}^2} - \frac{1}{(1-\varepsilon_{GR})^2 A_R^2}\right] \tag{11}$$

In Eq. (11), the ratio between the apparent contracted area for flow and the geometrical cross sectional area, respectively, is denoted as being an acceleration coefficient:

$$k_R = \frac{A_{Rc}}{A_R} \tag{12}$$

$$k_D = \frac{A_{Dc}}{A_D} \tag{13}$$

The acceleration coefficients at the entrance of riser (k_R) and downcomer (k_D), respectively, were introduced to account for the existence of non-uniform flow entrance regions and to quantify the entrance effects at the draft-tube ends caused by the apparent reduced flow area. Therefore, Eq. (11) can be written in the following form:

$$2gH_d = (\varepsilon_{GR} - \varepsilon_{GD}) = v_{SLR}^2 A_R^2 \left[\left(\frac{1}{k_R^2} - 1 \right) \times \frac{1}{A_R^2 (1-\varepsilon_{GR})^2} + \left(\frac{1}{k_D^2} - 1 \right) \frac{1}{A_D^2 (1-\varepsilon_{GD})^2} \right] \quad (14)$$

or in an explicit form as:

$$v_{SLR} = \left[\frac{2gH_d(\varepsilon_{GR} - \varepsilon_{GD})}{\left(\frac{1}{k_R^2} - 1 \right) \frac{1}{(1-\varepsilon_{GR})^2} + \left(\frac{1}{k_D^2} - 1 \right) \frac{A_R^2}{A_D^2} \frac{1}{(1-\varepsilon_{GD})^2}} \right]^{0.5} \quad (15)$$

From Eq. (15), it follows that knowledge of the average gas holdup in the riser and downcomer and the corresponding acceleration coefficients, k_R and k_D, does allow the prediction of the riser liquid superficial velocity in concentric-tube airlift reactors with gas sparged draft-tube. Also, for a given geometry of the airlift reactor, it is possible to determine the liquid circulation rate, Q_L [13]. These quantities are determined and verified in experimental concentric-tube airlift reactors of different scales, described below. As is reported in the literature [2,4], Eq. (15) also incorporates the diameter of the draft-tube in terms of the superficial liquid velocity in the riser. The riser diameter is a necessary geometric detail for the prediction of liquid velocity, because the ratio A_D/A_R does not uniquely define the reactor geometry [2]. The requirement of dimensional consistency is satisfied by Eq. (15), which may also be written in terms of liquid phase Froude number, expressed as [2]:

$$Fr_{LR}^2 = \frac{v_{SLR}^2}{gH_d} \quad (16)$$

3. Experimental

The linear liquid velocities and gas holdup in riser and downcomer, together with the pressure drops at the draft-tube ends were measured in a concentric-tube airlift reactor made of plexiglass. The nominal volume V_L was 0.070 m^3 (RIMP). Three different draft-tubes with inside diameters presented in Table 1 were used. Some studies were performed at different values of the bottom clearance (Table 1).

The proposed model for liquid circulation velocity was also verified in two larger concentric-tube airlift reactors made of stainless steel, having nominal volumes of 2.50 m^3 (RIS-1) and 5.20 m^3 (RIS-2), respectively. The reactors are shown schematically in Fig. 2a,b and their main geometric characteristics are given in Table 1.

Compressed air was supplied to RIMP through a perforated plate type sparger having 100 holes (diameter = 0.001 m). In RIS, air was introduced also through pipe spargers, with 300 holes (diameter = 0.0035 m). Air superficial velocities v_{SGR} ranged over 0.005–0.12 m/s. Tap water was used as the liquid phase, at 21 ± 1°C.

Table 1
Geometric characteristics of concentric-tube airlift reactors

Characteristic	Symbol	Unit	RIMP	RIS-1	RIS-2
Reactor diameter	D	m	0.200	0.600	0.900
Riser diameter	D_R	m	0.075	–	–
			0.100	–	–
			0.125	0.400	0.600
Bottom clearance	h_B	m	0.070	–	–
			0.160	–	–
			0.250	0.220	0.290
Top clearance	h_S	m	0	0	0
Gas-separator diameter	D_S	m	0.300	0.600	0.900
Gas-separator height	H_S	m	0.560	1.820	1.300
Draft-tube height	H_R	m	1.680	8.260	6.530
Liquid nominal volume	V_L	m^3	0.070	2.500	5.200

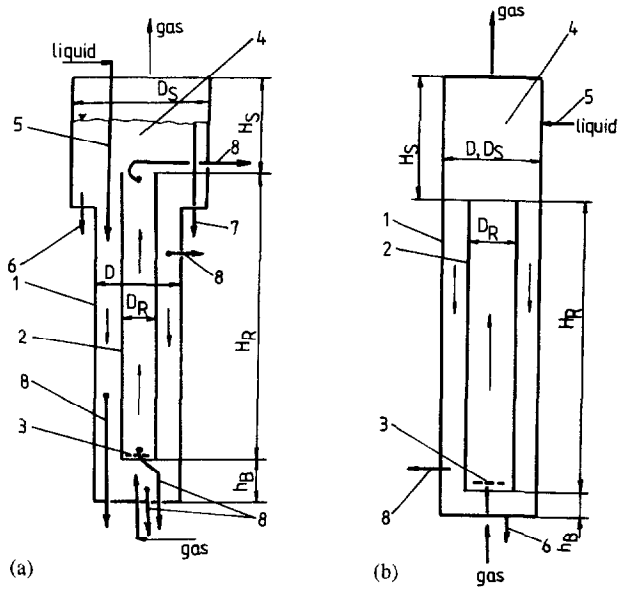

Fig. 2. Experimental set-up: (a) concentric-tube airlift reactor, nominal volume $V_L = 0.070$ m^3 (RIMP); (b) concentric-tube airlift reactor of larger volume ($V_L = 2.5$ m^3, (RIS-1); $V_L = 5.2$ m^3 (RIS-2)); (1) reactor body; (2) draft-tube; (3) gas sparger; (4) gas separator; (5) liquid feed pipe; (6) liquid exit; (7) liquid overflow; (8) pressure tap positions.

Pressure taps with hole diameter of 0.003 m were inserted into both the draft-tube and downcomer of RIMP and were connected to differential manometers. Air bubbles in the manometer lines were removed by frequently bleeding the system; pressure oscillations were dampened out by the insertion of capillary sections in the lines.

Liquid flow rates were measured in the downcomer by injecting a pulse of saturated NaCl solution (50 ml in RIMP and 200 ml in RIS). The tracer responses were detected at two points in the downcomer by electric conductivity probes [1,14]. The gas holdup in the riser and the downcomer was determined using the manometric method [2].

4. Results and discussion

4.1. Determination of acceleration coefficients

To calculate the acceleration coefficients k_R and k_D, linear liquid velocities and gas holdup were measured in the riser and downcomer sections of RIMP, together with pressure drops at the draft-tube ends, between the points 1–2 and 3–4, respectively (Fig. 1). In both the riser and downcomer, the pressure increases linearly with the column height, indicating average gas holdup according to Eqs. (3) and (4). The pressure variation is affected by the gas input, because liquid velocity changes are compensated by the change in static pressure.

Fig. 3 presents the variation of ΔP_B and ΔP_S with the gas superficial velocity in RIMP. It is evident from Fig. 3 that the larger pressure drop was obtained at the bottom draft-tube edge region, at a riser superficial velocity around 0.04 m/s. It was observed that with increasing gas velocity, gas bubbles converge to form a narrow path at the entrance to the riser, as Jones [5] also observed for different draft-tube diameters, phenomenologically supporting the existence of the entry zone, depicted as hatched area in Fig. 1. In this work, noticeable pressure differences between the inside and outside of the draft-tube were also observed at the top end of the draft-tube, as Wachi et al. [13] also reported. Other studies have reported negligible pressure differentials for the top zone [2,15,16]. For the most part, the variation of ΔP_S with v_{SGR} is opposite to that of ΔP_B (Fig. 3). This pressure rise opposes the direction of flow, especially at low gas throughput, thus, supporting the use of flow contraction rather than friction coefficients [7,13].

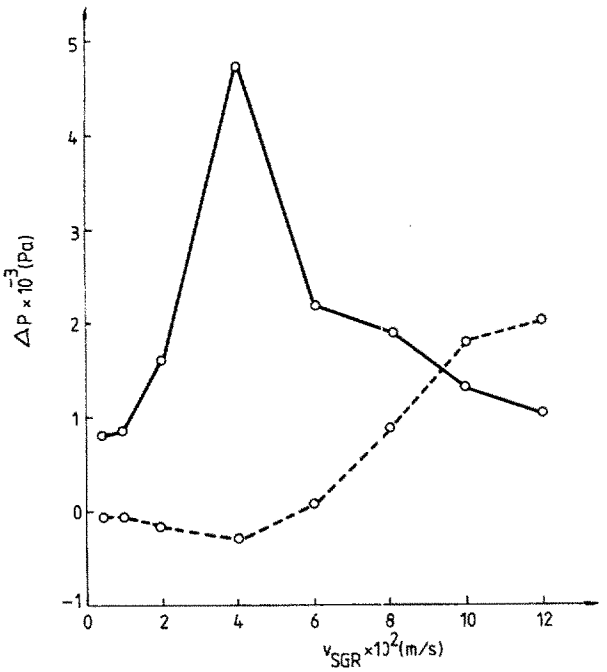

Fig. 3. Variation of pressure drops at the top and bottom zones with gas superficial velocity in RIMP ($h_B = 0.07$ m; $h_S = 0$; ——— ΔP_S; - - - ΔP_B.

Using the measured values of pressure drops, v_{LR}, v_{LD}, ε_{GR}, ε_{GD}, H_d, respectively in Eqs. (1)–(6), (12) and (13), the values of the acceleration coefficients were determined. The variation of k_R and k_D with the gas superficial velocity is shown in Fig. 4. This dependence of k_R and k_D on the gas superficial velocity is due to the influence of gas flow rate on gas holdup in riser and downcomer, that in turn determines circulation driving force. In addition, there is, as to an effect of v_{SGR} on v_{SLR}. For a given reactor geometry, the liquid circulation velocity, v_{SLR} can be specified by v_{SGR} and/or ε_G. Fig. 5a,b shows the variation of v_{SLR} with $\Delta\varepsilon_G$ and ε_{GT}, respectively. Here $\Delta\varepsilon_G$ instead of v_{SGR} is used as an independent variable since the liquid circulation is in principle driven by the difference $\Delta\varepsilon_G = \varepsilon_{GR} - \varepsilon_{GD}$. It is noted that an increase in gas holdup difference between the riser and downcomer results in a higher liquid circulation rate (Fig. 5a).

Also, the overall gas holdup is mainly determined by riser and downcomer gas holdup [2]:

$$\varepsilon_{GT} = \frac{A_R\varepsilon_{GR} + A_D\varepsilon_{GD}}{A_D + A_R} \tag{17}$$

From Fig. 5b, it is evident that the variation of v_{SLR} with ε_{GT} is similar with the dependence of v_{SLR} on the differential gas holdup between riser and downcomer.

In spite of the fact that v_{SLR} incorporates the influence of the reactor geometry and the operating parameter v_{SGR}, the acceleration coefficients can be correlated with ε_G and v_{SGR}. For the air–water system, the following functionality can be selected as a starting point for the correlations, i.e.:

$$k_i = f(v_{SGR}, \varepsilon_G) \tag{18a}$$

where the subscript i stands for either R or D.

The specific functional dependency of the acceleration coefficients on each variable was determined in the following manner.

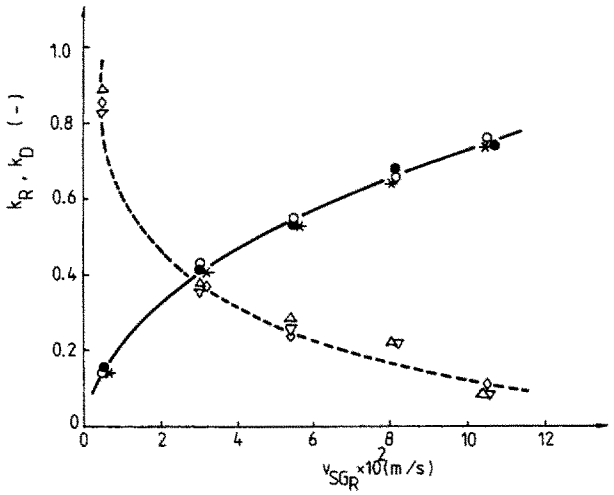

Fig. 4. Dependence of the acceleration coefficients on gas superficial velocity in RIMP (——— k_R: ○ $h_B = 0.07$ m; ● $h_B = 0.16$ m; * $h_B = 0.25$ m; - - - k_D: △ $h_B = 0.07$ m; ▽ $h_B = 0.16$ m; ◇ $h_B = 0.25$ m).

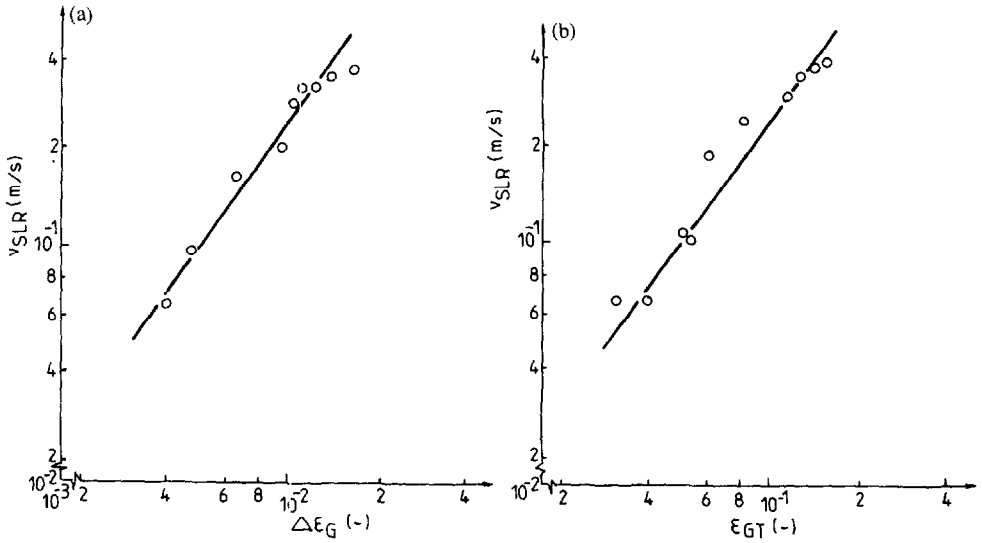

Fig. 5. (a) Dependence of the liquid superficial velocity in riser on differential gas holdup $\Delta\varepsilon_G = \varepsilon_{GR} - \varepsilon_{GD}$; (b) dependence of liquid superficial velocity in riser on the total gas holdup ε_{GT}; (RIMP; $h_S = 0$; $h_B = 0.25$ m; $D_R = 0.100$ m).

For constant volume of the continuous phase, the holdup of the dispersed phase was determined from the volumetric expansion on gas injection [17]. In our cylindrical reactor vessels, the volumes can be measured by the liquid level heights with (H_d) and without (H_L) gas input [18]. The dispersion liquid height was used as a measure of the dependence of k_i on gas holdup in the reactor. Based on the established theory of two-phase tube flow at the highest water flow rate in the draft-tube, it is estimated that the value of gas holdup so determined incorporates a small component due to the wall friction effects, of the order 10^{-3}. The overall gas holdup values obtained are in the range 0.03–0.17; thus, omission of the wall friction effect seems an acceptable approximation [12]. Also, by considering the effect of H_d on k_i, the influence of bottom clearance, that is the distance from the reactor bottom to the draft-tube lower edge, was also incorporated. The measurements performed at three values of bottom clearance, h_B, ($h_B = 0.07$ m; $h_B = 0.16$ m; $h_B = 0.25$ m), maintaining the top clearance (considered as the ungassed liquid height above the draft-tube) at a constant value ($h_S = 0$), demonstrated that the dispersion height did not depend on the bottom clearance, as is shown in Fig. 6. Owing to the fact that reactor geometry affects bubble entrainment [5], three different draft-tubes with inside diameter presented in Table 1 were used. Fig. 7 shows the static pressure profile measured by manometers along the column height in the riser and downcomer. In both airlift zones, the pressure increases linearly with the column height. Also, the pressure drop at the bottom increases in a significant measure with decreasing draft-tube diameter. Fig. 8 also illustrates the variation of the acceleration coefficients, determined experimentally, with gas superficial velocity for different draft-tube diameters. The contraction of the riser entry region is significantly enhanced by increasing the draft-tube diameter, as a consequence of the combination of high radial flow velocity at the bottom of the reactor and lower upward velocity inside the draft-tube.

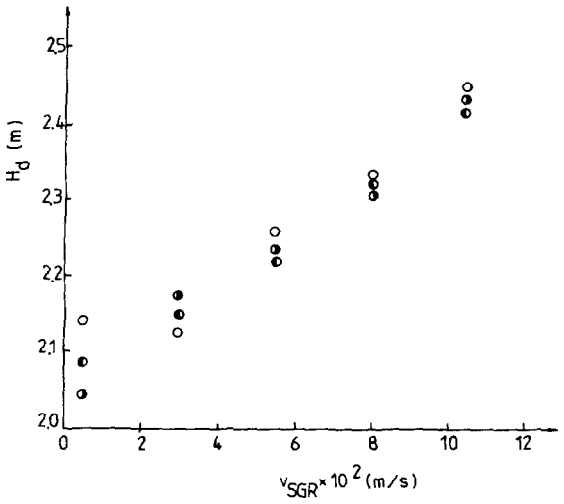

Fig. 6. Variation of dispersion height, H_d with gas superficial velocity, for different values of the bottom clearance, h_B ($h_S = 0$; $D_R = 0.100$ m; ○ $h_B = 0.07$ m; ◐ $h_B = 0.16$ m; ◑ $h_B = 0.25$ m).

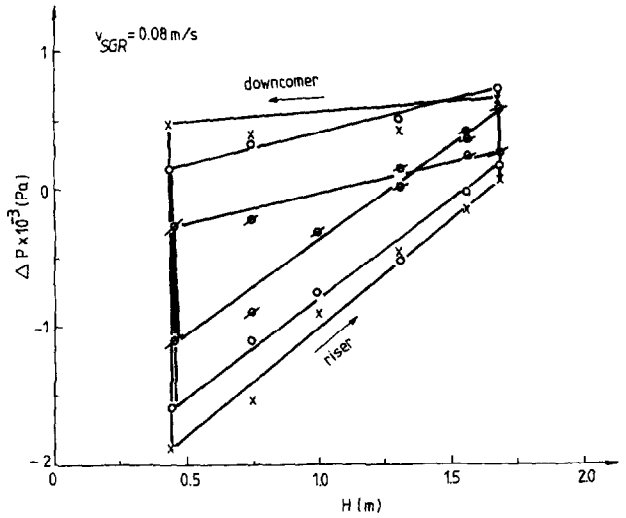

Fig. 7. Static pressure profiles in RIMP for different draft-tube diameters (× $D_R = 0.075$ m; ○ $D_R = 0.100$ m; ∅ $D_R = 0.125$ m).

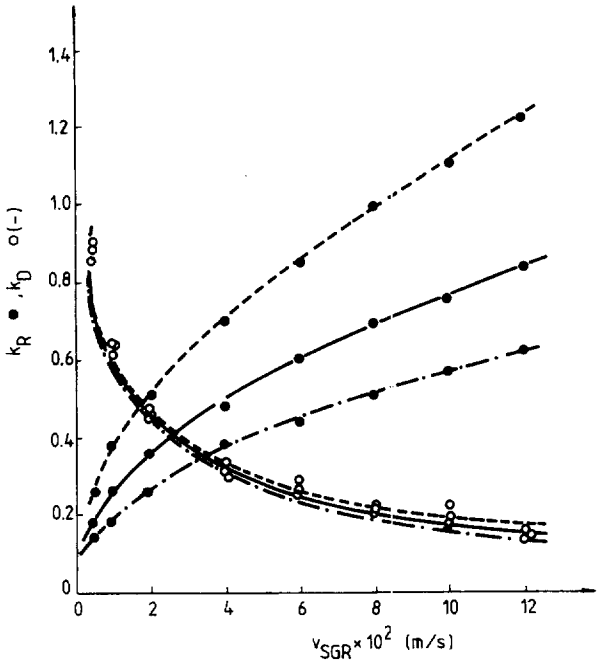

Fig. 8. Variation of k_R and k_D with draft-tube diameter (- - - $D_R = 0.075$ m; ——— $D_R = 0.100$ m; — · — $D_R = 0.125$ m; ● k_R; ○ k_B).

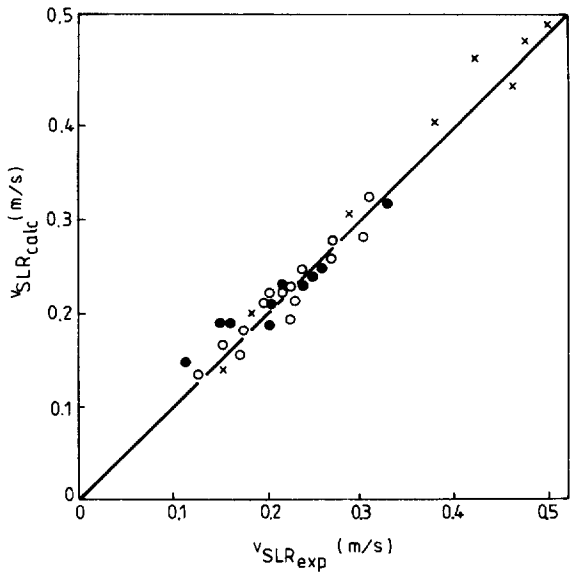

Fig. 9. Parity plot of experimentally values of v_{SLR} and those calculated with Eq. (15) with k_R and k_D obtained from the empirical models (Eqs. (18b) and (19)) (● RIS-1; ○ RIS-2; × Merchuk et al. [[3]]).

As is evident from Fig. 7, the pressure differences between the inside and the outside of the draft-tube observed at the top end of the inner column did not depend significantly on the draft-tube diameter, owing to the fact that the overflow velocities at the top zone, above the draft-tube do not differ significantly. Using coloured tracers, a rather similar flow pattern was observed at the top of the annulus for different draft-tube diameters. Hence, the acceleration coefficient at the downcomer entrance was found to be only weakly dependent on the draft-tube diameter, (Fig. 8). For all draft-tube diameters, entrained bubbles again produced some flow convergence in the downcomer entrance region.

The data were correlated using non-linear regression to obtain the following empirical equations:

$$k_R = 0.0535\, v_{SGR}^{0.44}\, H_d^{0.67} (D_R^2)^{-0.67} \quad r^2 = 0.896 \qquad (18b)$$

$$k_D = 0.21\, v_{SGR}^{-0.44}\, H_d^{-1.25} \quad r^2 = 0.908 \qquad (19)$$

From Eqs. (18b) and (19), it is evident that the acceleration coefficients do not have constant values for all operating conditions ($k_R \approx v_{SGR}^{0.44}$). The acceleration coefficient at the riser entrance should also be considered as scale-dependent ($k_R \approx D_R^2$), and determined by the reactor voidage ($k_R \approx H_d^{0.67}$), together with the effective flow path at the riser entrance, thereby, further affecting riser liquid circulation rates in a complex interaction between operating and geometrical parameters.

In the correlation proposed for the acceleration coefficient at the downcomer entrance (Eq. (19)), the exponent of D_R was found to be negligible by regression analysis. The increase in v_{SGR} and ε_G produces a turbulent flow pattern at the downcomer entrance and the contraction of the downcomer entrance cross flow area is the same relatively for the three draft-tubes. This is contrary to the riser entry region behaviour, where flow converges to form a narrower path as the draft-tube diameter decreases.

4.2. Application of the proposed model

The correlations Eqs. (18b) and (19) were applied together with the proposed model for v_{SLR} (Eq. (15)), to evaluate the liquid superficial velocity in the riser section of RIS-1 and RIS-2. The calculated v_{SLR} values in RIS-1 and RIS-2 were compared with the measured values (Fig. 9). The maximum deviation was ±28%, but the majority of the experimental v_{SLR} values could be predicted with an average error of ±10% for gas superficial velocities over 0.06 m/s (i.e., in the churn-turbulent flow regime). Fig. 9 also compares the predictions of Eqs. (15), (18b) and (19) with the experimental data obtained from the pressure drop measurements performed by Merchuk et al. [3]. Evidence suggests that the proposed model can reasonably predict the liquid circulation rates in concentric-tube airlift reactors when gas holdup values and reactor geometry are known.

5. Conclusions

A liquid circulation model for draft-tube sparged concentric-tube airlift reactors was developed using an energy balance over the circulation loop.

The pressure distributions measured along both the riser and downcomer in this study can provide direct, reliable estimates of pressure drops at the riser and downcomer entrances, which in turn were utilized in the energy balances to quantify deviations from ideal flow, at the entrance to the riser and downcomer. Apparent contraction of flow cross-

sections at the entrance of the draft-tube and annulus were accounted for through acceleration coefficients. The coefficients were experimentally determined and correlated with the riser gas superficial velocity, the dispersion height and the draft-tube diameter. The riser acceleration coefficient for the air–water system investigated decreases with increasing draft-tube diameter, while the corresponding downcomer contraction coefficient shows a weak dependence on draft-tube diameter. The bottom clearance effect was incorporated in the voidage effect, through the dispersion height.

The proposed model was shown to predict successfully the liquid circulation velocity in devices operating with water. The model was applied to several scales of concentric-tube airlift reactor. The influence of airlift geometry—dispersion height, riser-to-downcomer cross sectional areas ratio and flow areas at downcomer and riser entrances—was also revealed. The range of application of the model were broad: almost 50-fold variation in liquid circulation velocity, more than four-fold change in reactor height and three-fold increase in riser-to-downcomer cross-sectional area ratio. These broad ranges point to the usefulness of the model as a scale-up tool.

Appendix A. Nomenclature

A_D	Downcomer cross sectional area (m^2)
A_{Dc}	Apparent contracted cross sectional area at downcomer entrance (m^2)
A_R	Riser cross sectional area (m^2)
A_{Rc}	Apparent contracted cross sectional area at riser entrance (m^2)
D	Reactor diameter (m)
D_R	Riser diameter (m)
D_S	Gas-separator diameter (m)
Fr_{LR}	Froude number of liquid phase in riser (−)
g	Gravitational acceleration (m/s^2)
H_d	Dispersion height (m)
H_R	Draft-tube height (m)
H_S	Gas-separator height (m)
h_B	Bottom clearance (distance from reactor bottom to lower edge of draft tube) (m)
h_S	Top clearance (distance between ungassed liquid surface and top edge of draft tube) (m)
k_D	Acceleration coefficient at downcomer entrance (−)
k_R	Acceleration coefficient at riser entrance (−)
P_{DB}	Static pressure in the annulus at the bottom of downcomer (Pa)
P_{DS}	Static pressure in the annulus at the top of downcomer (Pa)
P_{RB}	Static pressure in draft-tube at the bottom of riser (Pa)
P_{RS}	Static pressure in draft-tube at the top of riser (Pa)
Δ_{PB}	Pressure drop at the bottom of the reactor (Pa)
Δ_{PS}	Pressure drop at the top of the reactor (Pa)
Q_L	Volumetric flow rate of liquid phase (m^3/s)
V_L	Liquid nominal volume of liquid phase (m^3)
$v_{D\alpha}$	Linear liquid velocity in the apparent contracted flow section at the downcomer entrance (m/s)
v_D, v_{LD}	Linear liquid velocity in the downcomer (m/s)
$v_{R\alpha}$	Linear liquid velocity in the apparent contracted flow section at the draft-tube entrance (m/s)
v_R, v_{LR}	Linear liquid velocity in the riser (m/s)
v_{SGR}	Gas superficial velocity in riser (m/s)
v_{SLD}	Liquid superficial velocity in downcomer (m/s)
v_{SLR}	Liquid superficial velocity in riser (m/s)

Greek letters

ε_{GD}	Downcomer gas holdup (−)
ε_{GR}	Riser gas holdup (−)
ε_{GT}	Overall gas holdup (−)
ρ	Liquid density (kg/m^2)

References

[1] M. Gavrilescu, R.Z. Tudose, Bioprocess Eng. 14 (1995) 33.
[2] M.Y. Chisti, Airlift Bioreactors, Elsevier, London, 1989.
[3] J.C. Merchuk, N. Ladwa, A. Cameron, M. Bulmer, A. Pickett, AIChE J. 40 (1994) 1105.
[4] Y. Chisti, M. Moo-Young, Improve the performance of airlift reactors, Chem. Eng. Prog., June (1993) 38.
[5] A.G. Jones, Chem. Eng. Sci. 40 (1985) 449.
[6] Y.C. Hsu, M.P. Dudukovic, Chem. Eng. Sci. 35 (1980) 135.
[7] Y. Chisti, B. Hallard, M. Moo-Young, Chem. Eng. Sci. 43 (1988) 451.
[8] Y. Chisti, M. Moo-Young, J. Chem. Technol. Biotechnol. 42 (1988) 211.
[9] P. Verlaan, Modelling and characterization of an airlift-loop bioreactor, PhD Thesis, University of Wageningen, 1987.
[10] J.A. Geurst, Int. J. Multiphase Flow 17 (1991) 815.
[11] E. Garcia Calvo, Chem. Eng. Sci. 44 (1989) 321.
[12] K. Akita, O. Nakanishi, K. Tsuchiya, Chem. Eng. Sci. 49 (1994) 2521.
[13] S. Wachi, A.G. Jones, T.P. Elson, Chem. Eng. Sci. 46 (1991) 657.
[14] M. Gavrilescu, R.Z. Tudose, Chem. Eng. Commun. 156 (1996) 89.
[15] W. Freedman, J.F. Davidson, Trans. Inst. Chem. Eng. 47 (1969) T251.
[16] K. Koide, S. Iwamoto, Y. Takasaka, S. Matsuura, E. Takahashi, M. Kimura, H. Kubota, J. Chem. Eng. Jpn. 17 (1984) 611.
[17] J. Philip, J.M. Proctor, K. Niranjan, J.F. Davidson, Chem. Eng. Sci. 45 (1990) 651.
[18] A. Lubbert, Characterization of bioreactors, in: K. Schuegerl (Ed.), Biotechnology, Vol. 4, VCH, Weinheim, 1991, p. 107.